EPJ manuscript No.
(will be inserted by the editor)

Collective 2_1^+ excitations in ^{206}Po and ^{208,210}Rn

T. Grahn[1,2a], J. Pakarinen[1,2,10], L. Jokiniemi[1], M. Albers[3], K. Auranen[1,2b], C. Bauer[4], C. Bernards[5], A. Blazhev[3], P. A. Butler[6], S. Bönig[4], A. Damyanova[7], T. De Coster[8], H. De Witte[8], J. Elseviers[8], L. P. Gaffney[6,8,9], M. Huyse[8], A. Herzáň[1,2], U. Jakobsson[1,2], R. Julin[1,2], N. Kesteloot[8], J. Konki[1,2], Th. Kröll[4], L. Lewandowski[3], K. Moschner[3], P. Peura[1,2], M. Pfeiffer[3], D. Radeck[3], P. Rahkila[1,2], E. Rapisarda[8,10], P. Reiter[3], K. Reynders[8], M. Rudiger[3], M.-D. Salsac[11], S. Sambi[8], M. Scheck[4,9], M. Seidlitz[3], B. Siebeck[3], T. Steinbach[3], S. Stolze[1,2], J. Suhonen[1], P. Thoele[3], M. Thürauf[4], N. Warr[3], P. Van Duppen[8,10], M. Venhart[12], M. J. Vermeulen[13], V. Werner[5,4], M. Veselsky[12], A. Vogt[3], K. Wrzosek-Lipska[8], and M. Zielińska[11]

[1] University of Jyvaskyla, Department of Physics, P.O. Box 35, FI-40014 University of Jyvaskyla, Finland
[2] Helsinki Institute of Physics, P.O. Box 64, FI-00014, Helsinki, Finland
[3] Institut für Kernphysik, Universität zu Köln, 50937 Köln, Germany
[4] Institut für Kernphysik, TU Darmstadt, 64289 Darmstadt, Germany
[5] Wright Nuclear Structure Laboratory, Yale University, P.O. Box 208120, New Haven, CT 06520-8120, U.S.A.
[6] Department of Physics, Oliver Lodge Laboratory, University of Liverpool, Liverpool, L69 7ZE, United Kingdom
[7] Université de Genève, 24 Quai Ernest-Ansermet, CH-1211 Genève 4, Switzerland
[8] Instituut voor Kern- en Stralingsfysica, Department of Physics, KU Leuven, 3001 Leuven, Belgium
[9] School of Engineering, University of the West of Scotland, Paisley PA1 2BE, UK
[10] CERN-ISOLDE, PH Department, CERN, CH-1211 Geneva 23, Switzerland
[11] CEA-Saclay, 91191 Gif-sur-Yvette, France
[12] Institute of Physics, Slovak Academy of Sciences, Dubravska cesta 9, 845 11 Bratislava 45, Slovak Republic
[13] Department of Physics, University of York, Heslington, York, YO10 5DD, United Kingdom

Received: date / Revised version: date

Abstract. In the present study, $B(E2; 2_1^+ \rightarrow 0_1^+)$ values have been measured in the ^{208,210}Rn and ^{206}Po nuclei through Coulomb excitation of re-accelerated radioactive beams in inverse kinematics at CERN-ISOLDE. These nuclei have been proposed to lie in, or at the boundary of the region where the seniority scheme should persist. However, contributions from collective excitations are likely to be present when moving away from the $N = 126$ closed shell. Such an effect is confirmed by the observed increased collectivity of the $2_1^+ \rightarrow 0_1^+$ transitions. Experimental results have been interpreted with the aid of theoretical studies carried out within the BCS-based QRPA framework.

PACS. 21.10.Ky Electromagnetic moments – 21.60.Ev Collective models – 23.20.Js Multipole matrix elements – 25.70.De Coulomb excitation – 27.80.+w $190 \leq A \leq 219$ – 29.38.Gj Reaccelerated radioactive beams

1 Introduction

One of the most fundamental concepts in nuclear structure are the magic numbers that are defined by the shell structure [1]. The tendency of like nucleons to pair to $I^\pi = 0^+$ drives nuclei with magic proton and neutron numbers to a more bound state than their immediate neighbours. The nuclei with magic proton and/or neutron number, such as the $N = 126$ isotones, can be reasonably well described with the nuclear shell model.

One of the successful models based on the excitations of unpaired nucleons to the shell-model orbitals is the seniority scheme [2]. If the valence nucleons reside at relatively high-j orbitals ($j \geq 7/2$), the seniority ν, which is the number of unpaired nucleons, can be regarded as a good quantum number. In the even-mass $N = 126$ isotones with $Z \geq 82$ the valence protons occupy the $1h_{9/2}$ single-particle orbital. Indeed, the energies of low-lying levels up to $I^\pi = 8_1^+$ can be well described as $\pi 1h_{9/2}$ $\nu = 2$ structures within the generalized seniority scheme [3]. The isomeric nature of the 8_1^+ states is characterized by the low energy of the $8_1^+ \rightarrow 6_1^+$ transitions. In the generalized seniority scheme these transitions, as well as all transitions in the ground-state band down to the $4_1^+ \rightarrow 2_1^+$ transition are seniority-conserving transitions between the $\nu = 2$ states. The $B(E2)$ values of the seniority-conserving transitions follow a parabolic trend with their minimum at the mid-j shell. The $2_1^+ \rightarrow 0_1^+$ transitions are senior-

[a] email: tuomas.grahn@jyu.fi
[b] Present address: Argonne National Laboratory, USA

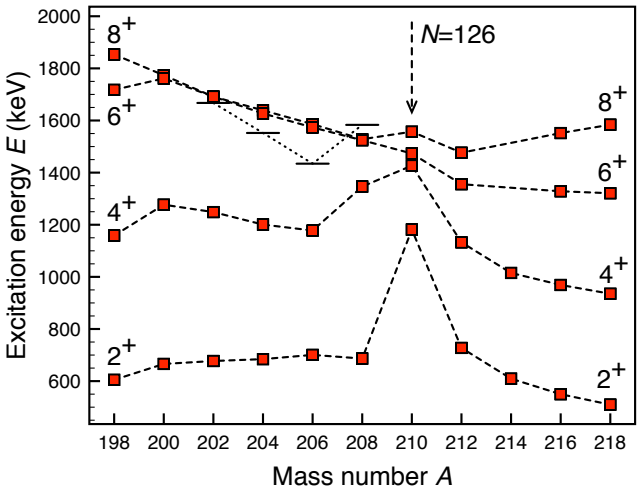

Fig. 1. Low-spin level-energy systematics of yrast states in Po nuclei. The 4_2^+ states are marked with a horizontal line. The data have been extracted from Ref. [4].

ity changing since the 0^+ ground states are $\nu = 0$ states and, therefore, the $B(E2; 2_1^+ \rightarrow 0_1^+)$ values should follow a different trend compared to the seniority-conserving transitions. Hence, in the generalized seniority scheme the $B(E2)$ values of the seniority-changing transitions are at their maximum at the mid-j shell.

However, when adding or removing protons/neutrons from a closed shell configuration, the particles/holes in the open shell start to interact via the quadrupole part of the residual interaction. Such a contribution is first observed for the low-spin states. This effect is clearly observed in the low-spin level-energy systematics as presented in Fig. 1 for the polonium isotopes. Immediately outside the $N = 126$ shell closure the energies of the 2_1^+ states decrease, followed by the 4_1^+ states when moving toward the lighter nuclei. The 2_1^+ level energies remain remarkably constant until the intruder states start to set in at around $N = 114$ when moving closer to the neutron mid shell at $N = 104$ [5,6].

In Ref. [7] the structure of neutron-deficient trans-Pb nuclei close to $N = 126$ has been discussed in terms of the seniority structures. However, as concluded in Ref. [8], the generalised seniority scheme with realistic interactions is inadequate to describe open-shell nuclei. In Ref. [9] simple shell-model calculations have been carried out for ^{208}Rn, in which two competing 4^+ states were predicted, one originating from a proton $\nu = 2$ multiplet and one from a neutron-hole configuration. In addition, the 2_1^+ states were assigned as neutron-hole excitations. In fact, the 4_2^+ states have been observed in Po (horizontal lines in Fig. 1) and Rn nuclei (see, e.g., Ref. [9] for ^{208}Rn) nuclei close to $N = 126$ as predicted by calculations [9].

In order to investigate the nature and collectivity of the 2_1^+ states near the $N = 126$ shell closure in ^{206}Po and ^{208,210}Rn, Coulomb-excitation measurements of radioactive ion beams in inverse kinematics were carried out at CERN-ISOLDE. In the present paper, the results and their impact on the understanding of the nuclear structure of the low-spin states near the $N = 126$ and $Z = 82$ closed shells are described.

2 Experiments

The radioactive ^{206}Po and ^{208,210}Rn nuclei were produced at CERN-ISOLDE [10] by bombarding an uranium carbide (UC_x) primary target with 1.4 GeV protons delivered by the PS Booster. The ^{206}Po beam was in fact extracted from the ISOLDE target after the proton irradiation stopped as the half-life of ^{206}Po is 8.8 days, which allowed sufficient yield for the present experiment from ^{206}Po activity accumulated during the previous irradiations of the primary target. Polonium atoms were ionized using the resonant-ionisation laser ion source (RILIS) [11] and mass selected by the ISOLDE High Resolution Separator (HRS). Radon atoms produced on-line at ISOLDE were ionized in the plasma ion source with the cooled Ta transfer line, and subsequently mass selected with the ISOLDE General Purpose Separator (GPS). After mass selection the ^{206}Po and ^{208,210}Rn nuclei were injected into the REX-ISOLDE post-accelerator complex [12] consisting of the REX-TRAP penning trap, the REX-EBIS charge breeder and the REX linear accelerator. REX-TRAP was used to cool, bunch, and purify the beams. The beam bunches were injected into the REX-EBIS charge breeder that matched the mass-to-charge (A/q) ratio of the ions to be suitable for post-acceleration. The REX linear post-accelerator delivered 2.85 MeV/u and 2.82 MeV/u ^{206}Po and ^{208,210}Rn beams, respectively, to the target position of the MINIBALL γ-ray spectrometer [13]. The beam energies were well below the limit to fulfill the criterion of "safe" Coulomb excitation [14]. The radioactive ion-beam yields at the MINIBALL target position were $\sim 5.6 \cdot 10^5$ pps ($^{208}Rn^{50+}$) and $\sim 2.1 \cdot 10^5$ pps ($^{210}Rn^{51+}$). The initial yield of $^{206}Po^{49+}$ was $\sim 5.6 \cdot 10^5$ pps which decreased over the course of the measurement since ^{206}Po was extracted from the ion source without proton irradiation.

Coulomb excitation was performed using 2 mg/cm^2 thick ^{104}Pd and ^{114}Cd targets, respectively. The targets were chosen in a way that the excitation energy of the 2_1^+ state is not overlapping with the 2_1^+ state energies in the projectile nuclei, and is lower than the corresponding energies in the nuclei of interest in order to minimize the γ-ray background arising from the Compton scattering events. In addition, reaction kinematics allowed the separation of the target and projectile nuclei with the chosen targets. The MINIBALL γ-ray spectrometer consists of eight triple-cluster Ge detectors arranged in a close geometry around the target chamber. The present set up had a total photopeak efficiency of 7% for 1.3 MeV γ rays. MINIBALL was used to detect the γ rays de-exciting the states under investigation.

Both scattered projectiles and target recoils were detected using an annular double-sided silicon strip detector (CD) with 16 annular strips positioned downstream of the target. The present radioactive beams were found to be close to 100% pure by measuring the γ-ray spectra

with the RILIS laser set on and off in the case of ^{206}Po. When the RILIS laser was set off, virtually no events in the particle-gated γ-ray spectra were observed. Since RILIS was not employed in the extraction of the ^{208,210}Rn beams, the same method could not be applied. Instead, the beam composition was measured using the ionization chamber downstream of the target and by using β-decay data from the beam-dump Ge detector. Events corresponding only to the Rn nuclei of interest were observed.

Identification of the beam and target nuclei detected in the CD was possible since both the scattering angle and the deposited energy of the recoiling particles were measured. A coincidence condition of exactly two particles in the CD (scattered beam and target recoil) and at least one γ-ray in MINIBALL was imposed. Figure 2 shows the spectrum of particle energy deposited in the CD as a function of scattering angle in the laboratory coordinates. In Fig. 4 γ-ray spectra respective to the three angular ranges (high, middle, low) are shown.

The γ rays were recorded in coincidence with the two-particle events (i.e. the scattered beam and the target recoil) observed in the CD. As the reaction kinematics can be reconstructed from the angular and energy information of the events recorded with the CD, and the γ-ray detection angle is known, event-by-event Doppler correction for the γ-ray energies can be applied, as described in detail in Ref. [13]. The background subtraction of the γ-ray spectra were carried out by subtracting the number of γ rays gated by the random events in the spectrum of time differences between the γ-ray events observed by MINIBALL and the particle events recorded by the CD detector. The subtracted background was normalized by the widths of the time windows. A spectrum of the time difference between the events observed in MINIBALL and the CD in the ^{208}Rn experiment is shown in Fig. 3. The procedure for the background subtraction was similar for the other two experiments. Sample γ-ray energy spectra, gated by the two-particle events observed in the CD with the three centre-of-mass scattering intervals as shown by Fig. 2c) is shown in Fig. 4.

The γ-ray energy spectra in coincidence with the two-particle events in the CD were constructed similarly for ^{210}Rn and ^{206}Po. The sample spectra are shown in Figs. 5 and 6, respectively.

The transition probabilities were extracted from the measured γ-ray intensities according to the Coulomb-excitation theory. In order to extract matrix elements in the ^{206}Po and ^{208,210}Rn nuclei, the measured γ-ray intensities have to be converted to absolute Coulomb-excitation cross sections. The latter requires normalization to the excitation of the target nuclei with the known electromagnetic matrix elements. The Coulomb-excitation γ-ray intensities were extracted from the event-by-event Doppler-corrected γ-ray energy spectra as shown in Figs. 4, 5, and 6.

The data for each nuclei were subdivided into three independent groups, as illustrated by Fig. 2, each subdivision corresponding to low, middle and high scattering angles of the target nuclei observed with the CD. The angular ranges in the centre-of-mass coordinates are given in Table 1. The γ-ray intensity data, together with the known matrix elements of the target nuclei, were used as input for the GOSIA2 Coulomb-excitation code [14]. The literature data used in the Coulomb-excitation analysis are shown in Table 2. Note that the $2_1^+ \rightarrow 4_1^+$ excitation is not observed in the data, but it is necessary to be included it in the GOSIA2 analysis as a so-called buffer state. This does not have influence on the results as such but it is needed in the GOSIA2 analysis as discussed in Ref. [15]. Some of the preliminary results of the present data were shown in Ref. [17].

In the GOSIA2 analysis both the target and the projectile 2_1^+ excitations are treated simultaneously by minimizing the χ^2 function in parallel. In this way, the measured projectile γ-ray intensities, shown in Table 3, can be converted to absolute excitation cross sections using the measured target γ-ray intensities and known literature data, as described in detail in Ref. [15]. Two unknown matrix elements are needed to describe excitation of the projectile nucleus. Therefore, a two-dimensional χ^2 surface, in which the χ^2 value is plotted as a function of the transition (ME_{02}) and diagonal (ME_{22}) matrix elements was used in the analysis to find a global minimum corresponding to the solutions for both matrix elements. In Figs. 7, 8, and 9 such two-dimensional surfaces are shown for each nucleus of interest. The condition $\chi^2 < \chi^2_{\mathrm{min}} + 1$ is applied to the graphs that represent the 1σ error bars of the resulting matrix-element values. The final results can therefore be extracted from the global minimum of χ^2 and are listed in Table 4. There is a strong correlation between the two matrix elements involved in the excitation process and therefore a subdivision of data and the present analysis technique are necessary to extract the $B(E2)$ values [15]. The $B(E2)$ values are given for the depopulating $2_1^+ \rightarrow 0_1^+$ transition, according to the relation $B(E2; 2^+ \rightarrow 0^+) = \frac{1}{5} \times \langle 0^+ || \hat{M}(E2) || 2^+ \rangle^2$ (see Eq. 3-31 in Ref. [16]).

3 Theoretical investigations

A theory designed to describe collective excitations in spherical open-shell even-even nuclei is the quasiparticle random-phase approximation (QRPA) [21,22]. The QRPA approach is based on the Bardeen-Cooper-Schrieffer (BCS) quasiparticles that are obtained by solving the BCS equations of motion within a chosen single-particle model space [22]. In the present calculations the single-particle space consisted of 12 proton states ($0g_{9/2}$, $0g_{7/2}$, $1d_{5/2}$, $0h_{11/2}$, $1d_{3/2}$, $2s_{1/2}$, $0h_{9/2}$, $1f_{7/2}$, $0i_{13/2}$, $2p_{3/2}$, $1f_{5/2}$, $2p_{1/2}$, in ascending order of energy) and 13 neutron states ($0h_{9/2}$,$1f_{7/2}$, $0i_{13/2}$, $2p_{3/2}$,$1f_{5/2}$, $2p_{1/2}$,$1g_{9/2}$, $0i_{11/2}$, $0j_{15/2}$, $2d_{5/2}$, $3s_{1/2}$, $1g_{7/2}$, $2d_{3/2}$, in ascending order of energy). These single-particle spaces were chosen such that the respective proton and neutron Fermi energies were well contained inside the model space. The single-particle energies were obtained from a Coulomb-corrected Woods-Saxon potential with the fitted parametrization taken from Ref. [16]. The adopted two-nucleon interaction was the Bonn-A one-boson exchange potential transferred to nuclear matter by

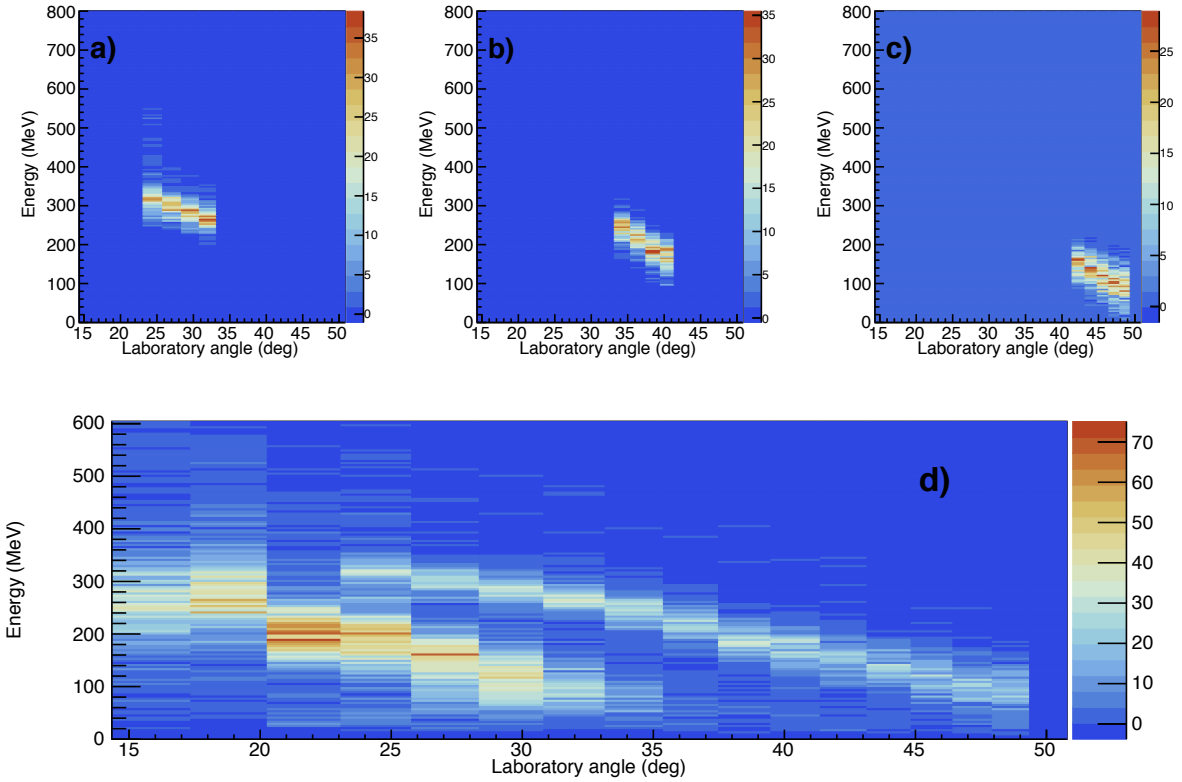

Fig. 2. Particle events following the Coulomb excitation of the ^{208}Rn beam on to the ^{114}Cd target as a function of the detection angle in the laboratory coordinates and the deposited energy detected in the CD (d). The target recoil (upper light region) and scattered beam (lower light region) components can be identified. Subfigures a, b and c show the gates set on the target recoils corresponding to the high, middle and low angular ranges of the beam recoils in the centre-of-mass coordinates, respectively.

Table 1. Intervals of scattering angles $\theta_i - \theta_j$ of the target recoils in the CD given in the centre-of-mass coordinates.

	$\theta_1 - \theta_2$ low strips 0-4 of the CD	$\theta_2 - \theta_3$ middle strips 5-8 of the CD	$\theta_4 - \theta_5$ high strips 9-12 of the CD
^{206}Po	$50.5° - 58.0°$	$41.9° - 50.5°$	$30.4° - 41.9°$
^{208}Rn	$43.9° - 51.9°$	$35.5° - 43.9°$	$25.0° - 35.5°$
^{210}Rn	$50.5° - 58.0°$	$41.9° - 50.5°$	$30.4° - 41.9°$

Table 2. Literature data used in the analysis. Note that for the level energies no errors were given in the GOSIA2 analysis. The data have been extracted from Refs [18,19,4,20].

	$E_{2_1^+}$ (keV)	$E_{4_1^+}$ (keV)	$\langle 0_1^+ \|\|\hat{M}(E2)\|\| 2_1^+ \rangle$ (eb)	$\langle 2_1^+ \|\|\hat{M}(E2)\|\| 2_1^+ \rangle$ (eb)
^{104}Pd	556	1324	0.73(2)	-0.61(15)
^{114}Cd	559	1284	0.714(21)	-0.46(3)

Table 3. Efficiency corrected γ-ray intensities measured in coincidence with two events in the CD for the projectile and target nuclei. Low, middle and high refer to the angular ranges given in Table 1.

	low		middle		high	
	projectile	target	projectile	target	projectile	target
^{206}Po	25(9)	164(22)	27(9)	147(21)	25 (9)	169(23)
^{208}Rn	136(15)	401(25)	130(14)	342(23)	120(14)	263(20)
^{210}Rn	95(17)	413(36)	103(18)	473(38)	108(18)	417(36)

the G-matrix techniques [23]. The two-nucleon potential was adapted to finite nuclei by a simple parametrization [24,25] where the pairing monopole matrix elements were scaled by one parameter for the protons and another one for the neutrons. These parameters were fixed by adjusting the lowest quasiparticle energies to the empirical pairing gaps obtained from the tabulated separation energies for protons and neutrons [26].

After solving the BCS equations the two-quasiparticle combinations were formed. These served as the building blocks for the QRPA matrices that were diagonalized in a standard way [22]. The particle-hole part of the two-nucleon interaction was adjusted to reproduce the experimental energy of the 2_1^+ state in the discussed ^{208,210}Rn and ^{206}Po nuclei in the way described in Refs. [24,25]. This adjustment guarantees the optimum collectivity of the 2_1^+ state from the theory point of view. After the adjustment the wave function of the 2_1^+ state is a coherent combination of two-quasiparticle pairs, a characteristic feature of a collective wave function [22]. The wave function obtained in this way can be used to produce a theoretical estimate of the reduced transition probability $B(E2)$ of an electric quadrupole transition from the 2_1^+ state to the ground state in a way as described in Ref. [22]. The $B(E2; 2_1^+ \rightarrow 0_1^+)$ value can be expressed in Weisskopf units (W.u.) [22] and it depends on the adopted effective charges for protons and neutrons. In the present calculations the bare charges, i.e. $1e$ for protons and $0e$ for neutrons were chosen. The corresponding computed results ($B(E2; 2_1^+ \rightarrow 0_1^+)$ values and diagonal matrix elements) are listed in the two last columns of Table 4.

Table 4. Experimental and theoretical results of the present work. The $\chi^2_{\rm tot}$ is defined as in [15], i.e. as a sum of χ^2 values corresponding to individual data points. The theoretical results are obtained within the QRPA approach.

	exp. $\langle 0_1^+\|\|\hat{M}(E2)\|\|2_1^+\rangle$ (eb)	exp. $\langle 2_1^+\|\|\hat{M}(E2)\|\|2_1^+\rangle$ (eb)	$\chi^2_{\rm tot}$	exp. $B(E2;2_1^+\rightarrow 0_1^+)$ (e^2b^2)	exp. $B(E2;2_1^+\rightarrow 0_1^+)$ (W.u.)	th. $B(E2;2_1^+\rightarrow 0_1^+)$ (W.u.)	th. $\langle 2_1^+\|\|\hat{M}(E2)\|\|2_1^+\rangle$ (eb)
^{204}Pb						3.23	-0.012
^{206}Po	$0.8^{+0.3}_{-0.2}$	$-2.0^{+4.0}_{-2.9}$	0.380	$0.13^{+0.10}_{-0.08}$	18^{+14}_{-10}	8.62	-0.079
^{206}Rn						7.94	-0.017
^{208}Rn	$0.70^{+0.14}_{-0.14}$	$2.2^{+3.1}_{-2.0}$	0.026	0.10(4)	13(6)	11.4	-0.035
^{210}Rn	$0.69^{+0.12}_{-0.12}$	$-0.07^{+3.00}_{-2.00}$	0.363	0.10(4)	13(6)	14.9	-0.058
^{212}Rn						4.92	-0.097
^{210}Ra						5.65	0.019

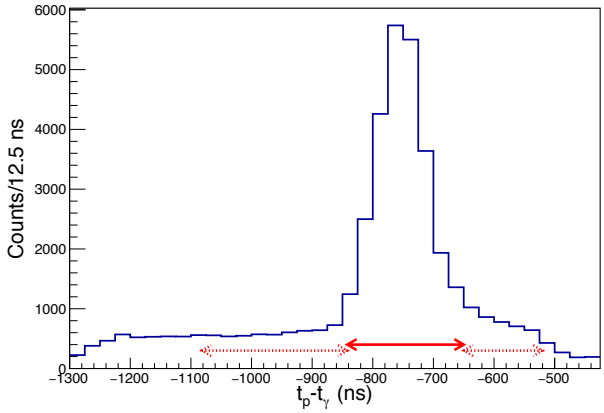

Fig. 3. Time difference histogram of γ rays observed in MINIBALL (t_γ) and particles in the CD (t_p) in the ^{208}Rn experiment. The solid red arrow marks the prompt coincidence time window and the dashed arrows show the random coincidence windows that are used for the background subtraction of the γ-ray energy spectra.

4 Discussion

4.1 $B(E2;2_1^+\rightarrow 0_1^+)$ values

Earlier studies of the transition probabilities in the $N = 122$ isotones have suggested that the seniority structures might persist in these isotopes even beyond the closed shells [27]. This was based on the hindered transition probability of the $8_1^+ \rightarrow 6_1^+$ transition. In Fig. 10 the partial level-energy systematics are plotted for the $N = 122$ isotones. Indeed, the low excitation-energy difference of the 8_1^+ and 6_1^+ states suggests a proton multiplet-type structure. However, the evolution of the 2_1^+ state energy suggests the opposite as it goes down in energy as a function of A. This is regarded as a sign of increasing collectivity.

In Fig. 11 the experimental $B(E2)$ values for the $2_1^+ \rightarrow 0_1^+$ and $8_1^+ \rightarrow 6_1^+$ transitions in the $N = 122$ isotopes have been plotted. The argument for the seniority structure arises from the hindered $8_1^+ + \rightarrow 6_1^+$ transition probabilities at mid-$j = 9/2$ proton sub shell. Such an evolution is indeed clearly visible and may indicate seniority structure at high spin. However, at low spin and in particular for the 2_1^+ states the structure is different. The measured $B(E2)$ values indicate moderate collectivity that sets in immediately when moving away from the closed proton shell.

The experimental and theoretical $B(E2;2_1^+ \rightarrow 0_1^+)$ values extracted in the present study for the $N = 122$ isotones under investigation have been plotted in Fig. 12 as a function of the proton number. The values follow a typical pattern when filling a sub shell. The $B(E2)$ value is at the minimum at the closed proton shell nucleus ^{204}Pb and increases towards the middle of the $\pi 0h_{9/2}$ sub shell. In these isotones the neutrons are occupying mainly the $1f_{5/2}$ sub shell and protons mainly the $0h_{9/2}$ sub shell immediately after ^{204}Pb. These sub-shell orbitals have $\Delta n = 1$, $\Delta\ell = 2$ and $\Delta j = 2$ being quadrupole partners and therefore proton-neutron interaction is moderately strong (see, e.g., [29]).

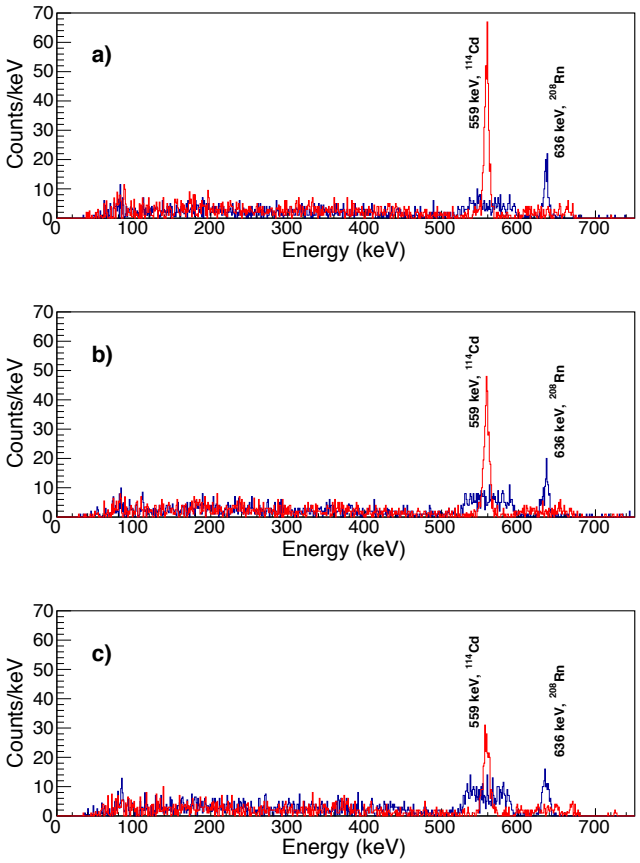

Fig. 4. Gamma-ray energy spectrum following Coulomb excitation of the ^{208}Rn beam impinging on the ^{114}Cd target, in coincidence with the two-particle events in the CD such that the target recoil is detected in the (a) high, (b) middle and (c) low angular range (cf. Fig. 2a), b) and c)). The event-by-event Doppler correction is performed for the target recoils (red) and for the scattered beam (blue).

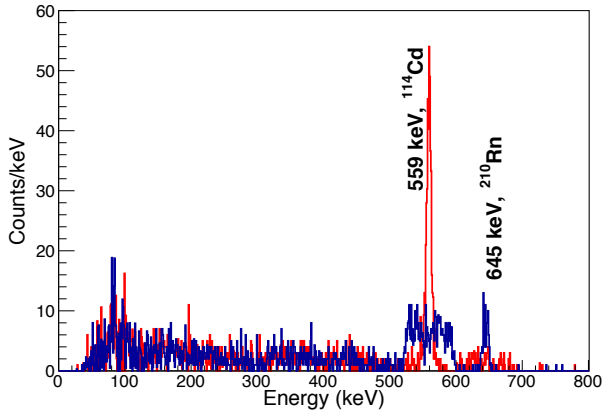

Fig. 5. Gamma-ray energy spectrum following Coulomb excitation of the ^{210}Rn beam impinging on the ^{114}Cd target, gated by the low centre-of-mass region ($50.5° - 58.0°$) of the CD (Fig. 2c). The event-by-event Doppler correction has been performed for ^{208}Rn (blue) and ^{114}Cd (red).

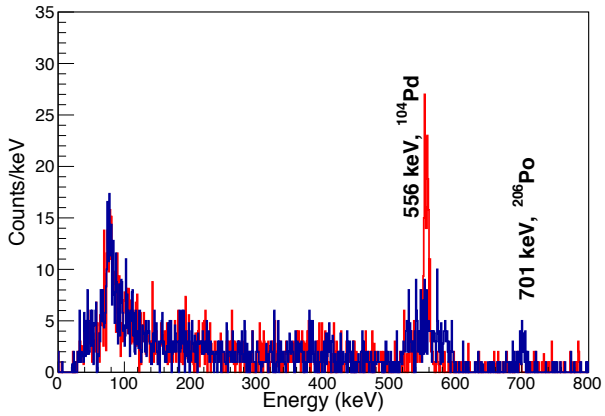

Fig. 6. Gamma-ray energy spectrum following Coulomb excitation of the ^{206}Po beam on to the ^{104}Pd target, gated by the high centre-of-mass region of the CD (c.f. Fig. 2a). The high centre-of-mass angular range of the CD is $30.4° - 41.9°$. The event-by-event Doppler correction has been performed for ^{206}Po (blue) and ^{104}Pd (red).

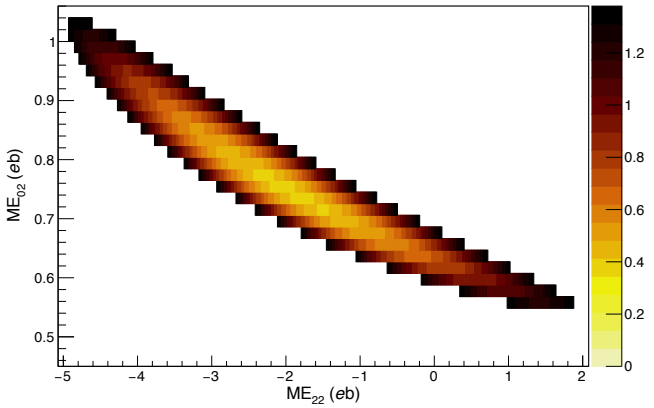

Fig. 7. Two-dimensional χ^2 surface as a function of diagonal $\langle 2^+||\hat{M}(E2)||2^+\rangle$ matrix element (denoted as ME$_{22}$) and transitional $\langle 0^+||\hat{M}(E2)||2^+\rangle$ matrix element (denoted as ME$_{02}$) The plotted surface is the region where $\chi^2 < \chi^2_{\rm min} + 1$ corresponding to the 1σ error bars [15]. The χ^2 scale is given on right.

In Fig. 13 the present experimental and theoretical $B(E2; 2_1^+ \rightarrow 0_1^+)$ values are plotted for the radon nuclei as a function of the mass number A. The theoretical $B(E2)$ value for the closed neutron-shell nucleus ^{212}Rn is very similar to that for the closed proton-shell nucleus ^{206}Pb. Immediately, when removing neutrons from the closed $N = 126$ $2p_{1/2}$ sub shell and entering into the $1f_{5/2}$ sub shell, the proton-neutron interaction starts to generate collectivity and thus increase the $B(E2)$ values. Evidence for this behaviour are from the high $B(E2)$ values, both experimental and theoretical, of the lighter Rn isotopes.

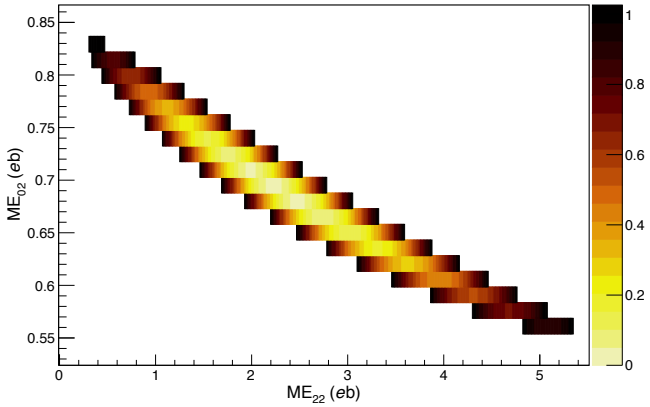

Fig. 8. Same as Fig. 7 but for ^{208}Rn.

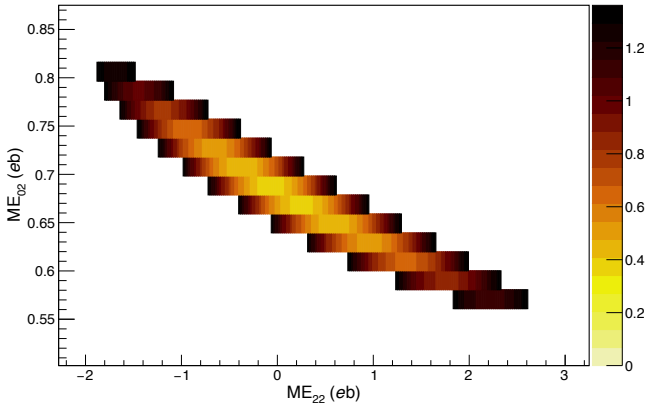

Fig. 9. Same as Fig. 7 but for ^{210}Rn.

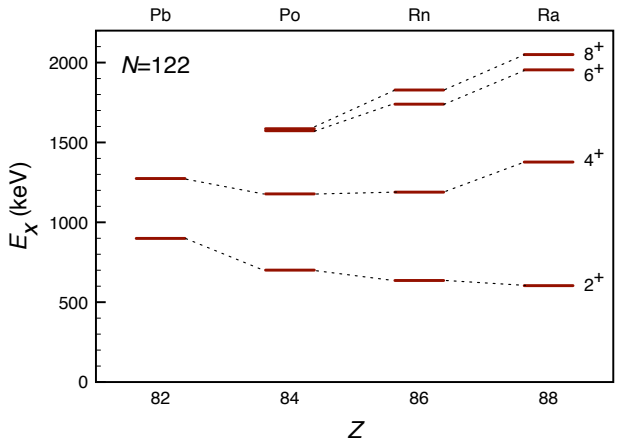

Fig. 10. Level-energy systematics of selected yrast states in the $N = 122$ isotones relevant to the present study. The data are extracted from [4].

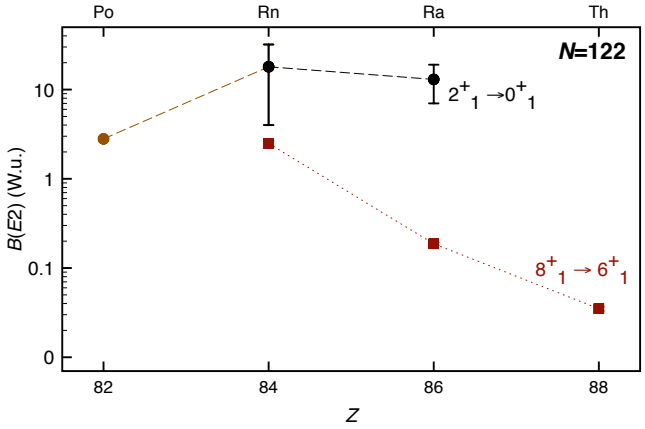

Fig. 11. Experimental $B(E2)$ values for the $2_1^+ \rightarrow 0_1^+$ and $8_1^+ \rightarrow 6_1^+$ transitions in the $N = 122$ isotopes. The data have been extracted from the present work (black symbols), from Ref. [27] and from References therein. For some of the data points the error bars are smaller than the symbol size.

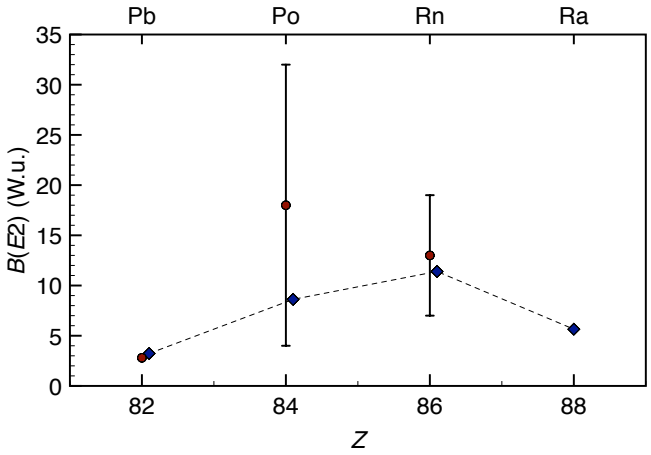

Fig. 12. The experimental (filled circles) and theoretical (filled diamonds) $B(E2; 2_1^+ \rightarrow 0_1^+)$ values in the $N = 122$ isotones ^{204}Pb, ^{206}Po, ^{208}Rn and ^{210}Ra extracted in the present work apart from the experimental value for ^{204}Pb ($Z = 82$), which has been taken from Ref. [28]. Some of the values are offset of their actual Z location for the clarity of the presentation.

4.2 Diagonal matrix elements

In the present work, only single-step excitations to the 2_1^+ states were observed both for the projectile and the target nuclei. The analysis method applied, described in detail in Ref. [15], in principle allows one to extract also the diagonal matrix elements of the 2_1^+ state. Since no additional data such as mean lifetime values exist for the nuclei under investigation, the present experiments are not very sensitive to the diagonal matrix elements, which results in large error bars as shown in Figs. 7, 8, and 9. On the basis of the vicinity of the closed neutron and protons shells at $N = 126$ and $Z = 82$ one could argue that the quadrupole moments of the 2_1^+ states would be close to zero. The present theoretical calculations suggest considerable collectivity

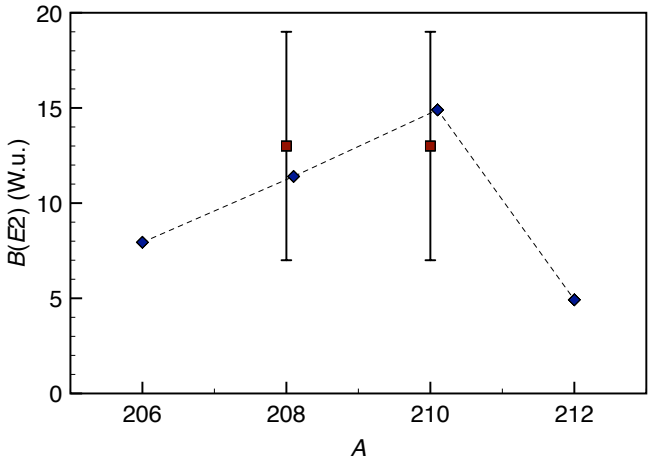

Fig. 13. The experimental (filled squares) and theoretical (filled diamonds) $B(E2; 2_1^+ \rightarrow 0_1^+)$ values obtained in the present work for the radon isotopes. Some of the values are offset of their actual A location for the clarity of the presentation.

of the $2_1^+ \rightarrow 0_1^+$ transitions, which indeed is observed, and, therefore, the zero quadrupole moments of the 2_1^+ states seem unjustified. The present Coulomb-excitation measurements, to a certain extent, suggest that the nuclei under investigation have non-vanishing quadrupole moments of the 2_1^+ state (see Table 4). In case of ^{208}Rn the quadrupole moment can be fixed to a positive value within 1σ confidence. However, in order to confirm this observation, complementary data are needed.

5 Conclusions

In the present work the Coulomb-excitation measurements of the radioactive ^{206}Po, ^{208,210}Rn beams in inverse kinematics have been carried out at CERN-ISOLDE. In addition, theoretical studies within the BCS-based QRPA calculations have been performed in this region of the nuclear chart. The data reveal the increased collectivity of the $2_1^+ \rightarrow 0_1^+$ transitions in these nuclei. Such an observation is also reproduced by the theory. While the higher-spin level patterns, namely the 8_1^+ state, suggest the presence of the seniority structures, the 2_1^+ state has a dominantly collective character which is likely to originate from an increase in proton-neutron interaction as the spatial overlap of the wave function gets stronger when entering the $1f_{5/2}$ and $0h_{9/2}$ sub shells for the neutrons and protons, respectively.

The authors acknowledge the support of the ISOLDE collaboration and technical teams and wish to acknowledge CSC – IT Center for Science, Finland, for computational resources. T. G. acknowledges the support of the Academy of Finland, contract 131665. A. V. acknowledges the support by the Bonn-Cologne Graduate School of Physics and Astronomy (BCGS). The present study was supported by IA-ENSAR (EU FP7 contract 262010), the Marie Curie Career Integration Grant (Grant No. 304033), the Academy of Finland (Grant No. 257562), U.S. DOE grant no. DE-FG02-91ER-40609, UK Science & Technology Facilities Council, BMBF grant no. 05P15RDCIA, FWO-Vlaanderen (Belgium), GOA/2010/010 (BOF KU Leuven), and the Interuniversity Attraction Poles Programme initiated by the Belgian Science Policy Office (BriX network P7/12).

References

1. Maria Goeppert Mayer, Physical Review **78**, 16 (1950)
2. Amos de-Shalit and Igal Talmi, *Nuclear Shell Theory* (Academic Press, New York, San Francisco, London, 1963) 283
3. Igal Talmi, Nuclear Physics **A172**, 1 (1971)
4. Data extracted from the NNDC ENSDF Online Data Service
5. N. Kesteloot *et al.*, Physical Review C **92**, 054301 (2015)
6. R. Julin, K. Helariutta and M. Muikku, Journal of Physics G: Nuclear and Particle Physics **27**, R109 (2001)
7. J. J. Ressler *et al.*, Physical Review C **69**, 034317 (2004)
8. M. A. Caprio, F. Q. Luo, K. Cai, Ch. Constantinou and V. Hellemans, Journal of Physics G: Nuclear and Particle Physics **39**, 105108 (2012)
9. W. J. Triggs, A. R. Poletti, G. D. Dracoulis, C. Fahlander and A. P. Byrne, Nuclear Physics **A395**, 274 (1983)
10. Erich Kugler, Hyperfine Interactions **129**, 23 (2000)
11. V. I. Mishin *et al.*, Nuclear Instruments and Methods in Physical Research **B73**, 550 (1993)
12. P. Van Duppen and K. Riisager, Journal of Physics G: Nuclear and Particle Physics **38**, 024005 (2011)
13. N. Warr *et al.*, European Physical Journal A **49**, 40 (2013)
14. T. Czosnyka, D. Cline, and C. Y. Wu, Bull. Am. Phys. Soc. **28**, 745 (1983)
15. M. Zielińska *et al.*, European Physical Journal A **52**, 99 (2016)
16. Aage Bohr and Ben R. Mottelson, *Nuclear Structure Volume I: Single-Particle Motion* (W. A. Benjamin Inc, New York, USA, 1969)
17. T. Grahn *et al.*, EPJ Web of Conferences **63**, 01009 (2013)
18. C. Fahlander *et al.*, Nuclear Physics A **485**, 327 (1988)
19. C. Fahlander, L. Hasselgren, and J. Thun, Nuclear instruments and methods **146**, 329 (1977)
20. S. Raman, C. Malarkey, W. Milner, C. Nestor, and P. Stelson, Atomic Data and Nuclear Data Tables **36**, 1 (1987)
21. M. Baranger, Physical Review **120**, 957 (1960)
22. J. Suhonen, *From Nucleons to Nucleus: Concepts of Microscopic Nuclear Theory* (Springer, Berlin, 2007)
23. K. Holinde, Physics Reports **68**, 121 (1981)
24. J. Suhonen, A. Faessler, T. Taigel and T. Tomoda, Physics Letters **B202**, 174 (1988)
25. J. Suhonen, T. Taigel and A. Faessler, Nuclear Physics **A486**, 91 (1988)
26. G. Audi, F. G. Kondev, M. Wang, B. Pfeiffer, X. Sun, J. Blachot and M. MacCormick, Chinese Physics **C36**, 1157 (2012)
27. J. J. Ressler *et al.*, Physical Review C **69**, 034331 (2004)
28. S. Raman, C.W. Nestor, P. Tikkanen, Atomic Data and Nuclear Data Tables, **78**, 1 (2001)
29. K. Heyde *et al.*, Nuclear Physics A **466**, 189 (1987)